Charged multiplicity distribution in pp interactions at CERN ISR energies

A. Breakstone,[a] R. Campanini,[b] H. B. Crawley,[a] G. M. Dallavalle,[b] M. M. Deninno,[b] K. Doroba,[f]
D. Drijard,[c] F. Fabbri,[c] M. A. Faessler,[c] A. Firestone,[a] H. G. Fischer,[c] H. Frehse,[c] W. Geist,[c]
G. Giacomelli,[b] R. Gokieli,[f] M. Gorbics,[a] C. Gruhn,[c] P. Hanke,[e] M. Heiden,[c] W. Herr,[e]
P. G. Innocenti,[c] E. E. Kluge,[e] J. W. Lamsa,[a] T. Lohse,[d] W. T. Meyer,[a] G. Mornacchi,[c]
T. Nakada,[e] M. Panter,[c] A. Putzer,[e] K. Rauschnabel,[d] B. Rensch,[e] F. Rimondi,[b] R. Sosnowski,[f]
E. Stenlund,[c] T. J. M. Symons,[c] M. Szczekowski,[c] R. Szwed,[f]
O. Ullaland,[c] D. Wegener,[d] and M. Wunsch[e]

[a]*Ames Laboratory and Physics Department, Iowa State University, Ames, Iowa*
[b]*Istituto di Fisica dell'Università and Istituto Nazionale di Fisica Nucleare, Bologna, Italy*
[c]*CERN, European Organization for Nuclear Research, Geneva, Switzerland*
[d]*Institut für Physik der Universität Dortmund, Dortmund, Germany*
[e]*Institut für Hochenergiephysik der Universität Heidelberg, Heidelberg, Germany*
[f]*University and Institute for Nuclear Studies, Warsaw, Poland*
(Ames-Bologna-CERN-Dortmund-Heidelberg-Warsaw Collaboration)
(Received 23 March 1984)

The multiplicities of charged secondaries in proton-proton collisions were determined using the split-field-magnet detector at the CERN Intersecting Storage Rings (ISR). Measurements are presented on multiplicity distributions both for inelastic and non-single-diffractive events at four different energies $\sqrt{s} = 30.4$, 44.5, 52.6, and 62.2 GeV. The results reported here represent the first high-statistics measurement of charged multiplicity distributions at ISR energies with a magnetic detector covering nearly the full solid angle.

I. INTRODUCTION

Most of the reliable data on multiplicity distributions at Fermilab, CERN ISR, and CERN SPS collider energies have been obtained by visual methods, i.e., bubble-chamber or streamer-chamber technique. Here we report on an experiment performed with an electronic detector, i.e., a set of multiwire proportional chambers inside the split-field-magnet (SFM) detector at the CERN ISR. The main advantage of nonvisual methods is the possibility of analyzing much larger event samples, but the resulting small statistical errors necessitate a thorough and lengthy study of possible systematic effects and errors. Another advantage over streamer-chamber experiments is the genuinely inclusive trigger used with the SFM. In this experiment a single charged particle anywhere in phase space is sufficient to trigger the detector, while in other experiments an external trigger, usually a left-right coincidence from counters in the forward direction, was used. Another advantage of the present experiment is the presence of a magnetic field, particularly in the region of the outgoing beams. Thus, particles produced at small angles in inelastic collisions, which normally remain inside the beam pipe, are swept out into the track chambers. We therefore present results on samples of both inelastic and non-single-diffractive events, which in the past have often not been clearly separated. These two classes of events exhibit a different dependence on energy, and a separation into these two categories turns out to be necessary in order to make meaningful comparisons with scaling concepts.

II. EXPERIMENT

The experiment was performed at the CERN ISR using the SFM detector to measure the momenta of all charged particles. Details on the setup and on the data acquisition have been described previously.[1] The layout of the SFM detector is given in Fig. 1.

With this setup, four samples of events were obtained at $\sqrt{s} = 30.4$, 44.5, 52.6, and 62.2 GeV by using the so-called "minimum-bias" trigger, which requires at least one track candidate be seen in the detector. From a Monte Carlo study we estimate that 95% of the inelastic pp cross section is accepted by the minimum-bias trigger, independent of magnetic field and c.m. energy. At these four energies the samples collected consisted of 37 069, 61 455, 26 842, and 58 196 events, respectively.

III. CORRECTIONS APPLIED TO THE DATA

Several effects cause small differences in our detector between the true and the observed multiplicities. We have corrected for K_S^0 and Λ decays, electron and positron contamination, and geometrical acceptance.

A. K_S^0 and Λ decays

The observed events are contaminated by charged secondary particles coming from K_S^0 mesons and Λ baryons which decay near the event origin. In order to determine correctly the higher-order moments of the multiplicity distribution, one cannot subtract this contamination globally but rather has to determine the average number of these secondary particles for each multiplicity. The decays of neutral strange particles were reconstructed explicitly.[2] This allowed a multiplicity-dependent correction for this contribution, which also took into account the reconstruction efficiency. The average number of K_S^0 and Λ decays per inelastic collision was 0.53 ± 0.03 and 0.18 ± 0.03, respectively.
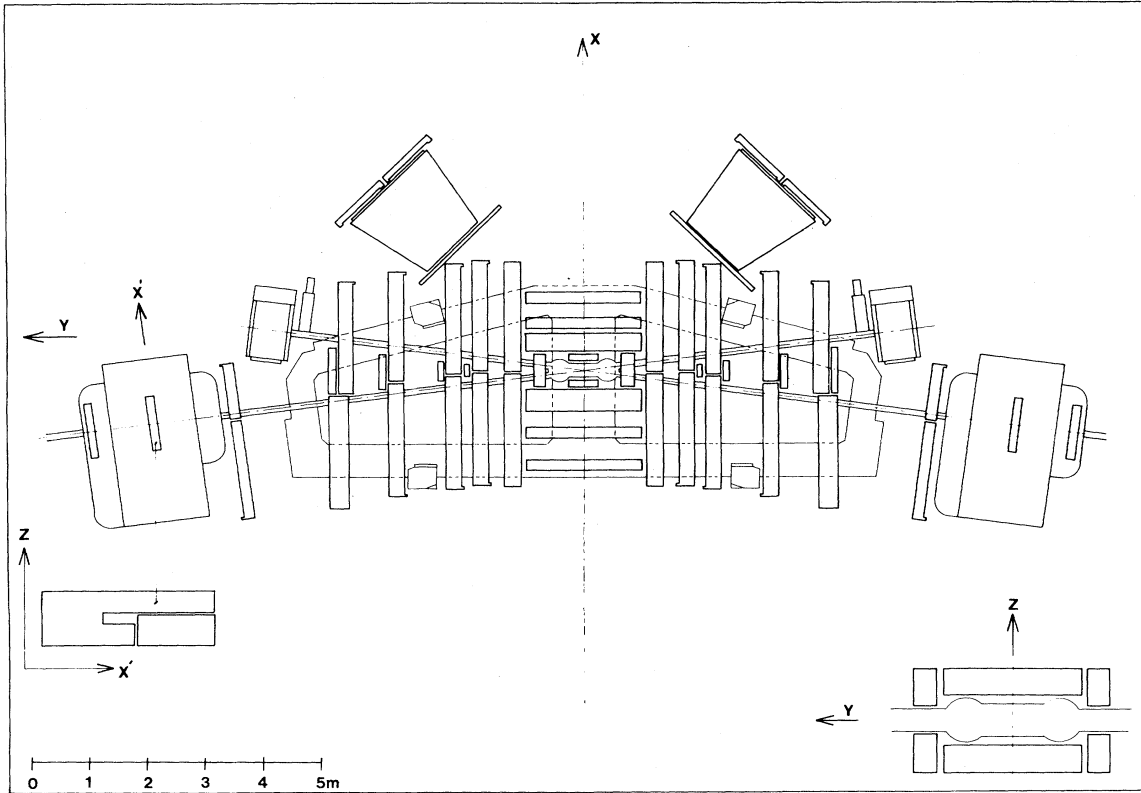
FIG. 1. The split-field-magnet detector at the CERN ISR: top view showing the layout of multiwire proportional chambers and the external apparatus for particle identification.

B. Electron and positron contamination

The events may contain an additional contamination of electrons and positrons coming primarily from the conversion of photons from π^0 decays in either the vacuum chamber or directly from Dalitz pairs. We have used a Monte Carlo method to evaluate this contamination. A sample of complete events with different multiplicities, including charged particles as well as π^0's, was generated, and the decay of the π^0 into either two photons or a single photon plus an electron-positron pair was simulated. The charged hadrons and the electrons and positrons coming from the Dalitz decay of the π^0 or from the conversion of the photons in the beam pipe were tracked through the magnetic field of the spectrometer. Using our standard programs to reconstruct these events, we have determined this contribution to the charged multiplicity as a function of the number of observed particles. This enables us to apply a multiplicity-dependent correction rather than just a global correction. On the average 0.45 ± 0.13 charged particles per event were determined to be electrons or positrons coming from π^0 decays.

C. Geometrical acceptance

To correct for losses due to the geometrical acceptance we have used two different methods. In the first case we proceeded as follows. If O_n is the number of events with n observed tracks (after corrections for neutral decays)

and T_m is the unknown true number of m-prong events produced, then

$$O_n = \sum_m P_{mn} T_m , \tag{1}$$

where P_{mn} is the probability to observe a true m prong as an event with n tracks.

To determine the matrix elements P_{mn} we have used a large number of simulated events, generated according to longitudinal phase space. Details about this simulation can be found in Ref. 3. For each event we have determined the number of tracks which would have been detected in the apparatus by simulating the detector and then applying the standard reconstruction programs. The constraint of charge conservation causes the coefficient P_{mn} to be different from zero only if m is an even number. The parameters T_m were determined by a least-squares method. We define E_n by

$$E_n = O_n - \sum P_{mn} T_m ,$$

and then minimize the function

$$M = \sum (E_n / \Delta E_n)^2$$

with respect to the parameters T_m. The quantity ΔE_n is the variance of E_n. The resulting minimum $M_{\min}$ is correctly distributed as a χ^2 distribution. In the second method, the acceptance table was applied directly to simulated events starting from the inclusive phase-space distri-

bution as measured in the experiment. The simulated input multiplicity distribution was varied until the acceptance-corrected output distribution agreed with the observed one.

The results obtained using these two methods were in good agreement. Our final corrected multiplicity distributions are the average of the distributions obtained by the two different methods.

IV. DIFFRACTIVE EVENTS

For the test on the scaling properties of multiplicity distributions it is necessary to take into account the differ-

ence behavior of the diffractive component in the multiparticle production. Using data on πp and Kp interactions, it has been shown[4] that the leading-particle effects are responsible for the nonuniversality of the classical Koba-Nielsen-Olesen (KNO) scaling behavior of the multiplicity distribution. For our analysis of the KNO scaling we use non-single-diffractive events only to take into account the different production mechanisms of diffractively produced events. By "non-single-diffractive" events we mean the sample of all inelastic events except those in which one of the incident protons, but not both of them, appears to undergo diffractive dissociation. In order to separate events produced by single diffraction, which

TABLE I. Topological cross sections (in mb).

N	30.4 GeV	44.5 GeV	52.6 GeV	62.2 GeV
		(a) Inelastic events		
2	2.22 ±0.42	1.76±0.33	1.74 ±0.33	1.68 ±0.35
4	4.84 ±0.63	3.76±0.46	3.84 ±0.47	3.35 ±0.54
6	5.01 ±0.50	4.39±0.40	3.88 ±0.41	3.69 ±0.54
8	5.09 ±0.41	4.76±0.38	3.92 ±0.35	4.04 ±0.50
10	4.62 ±0.42	4.60±0.34	4.45 ±0.32	4.12 ±0.33
12	3.77 ±0.28	4.28±0.35	4.33 ±0.27	3.98 ±0.25
14	2.72 ±0.24	3.39±0.27	3.62 ±0.18	3.60 ±0.25
16	1.96 ±0.18	2.77±0.21	2.87 ±0.16	3.05 ±0.20
18	1.23 ±0.13	1.73±0.14	2.32 ±0.14	2.40 ±0.17
20	0.69 ±0.11	1.24±0.09	1.60 ±0.11	1.91 ±0.13
22	0.44 ±0.07	0.78±0.06	1.01 ±0.09	1.30 ±0.10
24	0.20 ±0.08	0.52±0.06	0.65 ±0.05	1.04 ±0.08
26	0.11 ±0.06	0.33±0.07	0.38 ±0.05	0.66 ±0.07
28	0.05 ±0.03	0.16±0.05	0.23 ±0.05	0.39 ±0.08
30	0.02 ±0.01	0.08±0.03	0.15 ±0.03	0.16 ±0.03
32	0.003±0.003	0.03±0.02	0.11 ±0.03	0.15 ±0.03
34	0.003±0.003	0.02±0.02	0.06 ±0.03	0.07 ±0.03
36		0.02±0.02	0.04 ±0.03	0.05 ±0.03
38		0.01±0.01	0.01 ±0.01	0.010±0.007
40			0.007±0.005	0.004±0.003
42			0.002±0.002	
		(b) Non-single-diffractive events		
2	0.32 ±0.06	0.29±0.05	0.39 ±0.04	0.28 ±0.05
4	2.48 ±0.25	1.36±0.14	1.38 ±0.14	1.10 ±0.17
6	4.10 ±0.43	3.40±0.36	2.95 ±0.34	2.60 ±0.31
8	4.82 ±0.41	4.26±0.38	3.83 ±0.45	3.55 ±0.50
10	4.62 ±0.42	4.60±0.34	4.45 ±0.32	4.08 ±0.33
12	3.77 ±0.28	4.28±0.35	4.33 ±0.27	3.98 ±0.25
14	2.72 ±0.24	3.39±0.27	3.62 ±0.18	3.60 ±0.25
16	1.96 ±0.18	2.77±0.21	2.87 ±0.16	3.05 ±0.20
18	1.23 ±0.14	1.73±0.14	2.32 ±0.14	2.40 ±0.17
20	0.69 ±0.11	1.24±0.09	1.60 ±0.11	1.91 ±0.13
22	0.44 ±0.07	0.78±0.06	1.01 ±0.09	1.30 ±0.10
24	0.20 ±0.08	0.52±0.06	0.65 ±0.05	1.04 ±0.08
26	0.11 ±0.06	0.33±0.07	0.38 ±0.05	0.66 ±0.07
28	0.05 ±0.03	0.16±0.05	0.23 ±0.05	0.39 ±0.08
30	0.02 ±0.01	0.08±0.03	0.15 ±0.03	0.16 ±0.03
32	0.003±0.003	0.03±0.02	0.11 ±0.03	0.15 ±0.03
34	0.003±0.003	0.02±0.02	0.06 ±0.03	0.07 ±0.03
36		0.02±0.02	0.04 ±0.03	0.05 ±0.03
38		0.01±0.01	0.01 ±0.01	0.010±0.007
40			0.007±0.003	0.004±0.003
42			0.002±0.002	
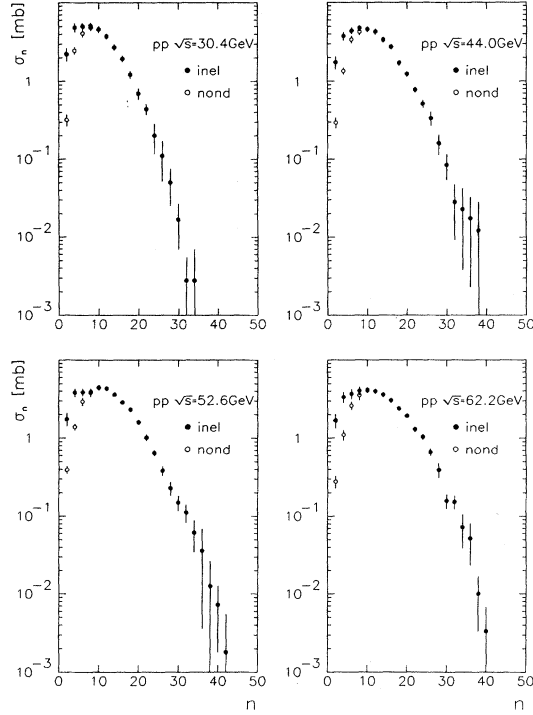
FIG. 2. Topological cross sections as a function of the charged-particle multiplicity for inelastic and non-single-diffractive events at different ISR energies.

plays an important role for low multiplicities, we have applied some kinematical cuts, which are based upon the typical topology of diffractive events. We assume an event to be of the diffractive type when either a single track was found in one of the two rapidity hemispheres with a Feynman x larger than 0.8 or if no track at all was found in one hemisphere. In the latter case we assume that the forward-scattered proton is too fast to leave the beam pipe and hence could not be detected. However, such an event was treated as nondiffractive if the total reconstructed multiplicity was larger than 7 (the diffractive component should give a substantial contribution only to the low-multiplicity part of the distribution). Using these cuts, around 15% of the events were determined to be diffractive at the four different energies. A study with simulated events showed that between 88 and 95% of the visible diffractive events were correctly classified as diffractive. More details about this procedure can be found in Ref. 3.

V. RESULTS

The topological cross sections of charged particles are given in Table I and are shown in Fig. 2 at center-of-mass energies of $\sqrt{s} = 30.4$, 44.5, 52.6, and 62.2 GeV. The distributions shown were normalized to the measured total inelastic cross sections at the different ISR energies.[5] Results are presented both for the sample of inelastic events (i.e., where elastic events were excluded) and of non-single-diffractive events, where additional cuts, mentioned

TABLE II. Moments of the multiplicity distribution.

	30.4 GeV	44.5 GeV	52.6 GeV	62.2 GeV
	(a) Inelastic events			
$\langle n \rangle$	9.43±0.18	10.86± 0.16	11.55± 0.171	12.25± 0.21
D_2	5.05±0.11	5.76± 0.10	6.23± 0.10	6.62± 0.10
D_3	4.56±0.17	5.20± 0.19	5.55± 0.20	5.65± 0.18
f_2	16.10±1.10	22.30± 1.10	27.30± 1.20	31.50± 1.40
f_3	37.00±8.70	63.10±13.20	77.60±15.50	74.00±15.00
γ_2	0.29±0.01	0.28± 0.01	0.29± 0.01	0.29± 0.01
γ_3	0.11±0.01	0.11± 0.01	0.11± 0.01	0.10± 0.01
C_2	1.29±0.02	1.28± 0.01	1.29± 0.01	1.29± 0.01
C_3	1.97±0.06	1.96± 0.05	1.98± 0.05	1.97± 0.05
C_4	3.44±0.17	3.41± 0.15	3.48± 0.15	3.40± 0.15
C_5	6.66±0.49	6.60± 0.45	6.81± 0.45	6.44± 0.41
	(b) Non-single-diffractive events			
$\langle n \rangle$	10.54±0.14	12.08± 0.13	12.76± 0.14	13.63± 0.16
D_2	4.75±0.11	5.39± 0.10	5.82± 0.10	6.16± 0.10
D_3	4.32±0.17	4.99± 0.20	5.33± 0.20	5.36± 0.17
f_2	12.03±0.94	17.00± 1.00	21.10± 1.10	24.30± 1.10
f_3	33.90±7.80	61.10±12.60	75.60±14.80	67.70±12.90
γ_2	0.20±0.01	0.20± 0.01	0.21± 0.01	0.20± 0.01
γ_3	0.07±0.01	0.07± 0.01	0.07± 0.01	0.06± 0.01
C_2	1.20±0.01	1.20± 0.01	1.21± 0.01	1.20± 0.01
C_3	1.68±0.03	1.67± 0.03	1.70± 0.03	1.67± 0.03
C_4	2.64±0.10	2.63± 0.01	2.70± 0.09	2.60± 0.08
C_5	4.58±0.28	4.59± 0.26	4.79± 0.25	4.43± 0.20
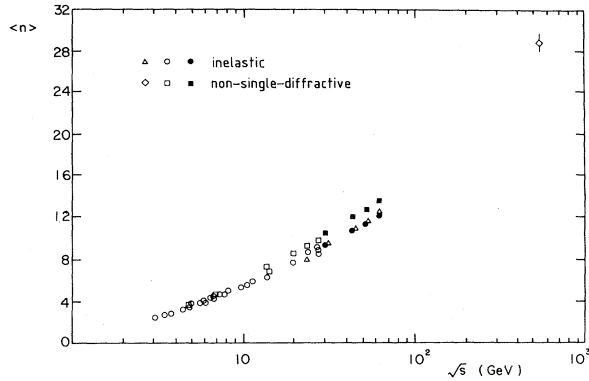
FIG. 3. Mean value of the charged-particle multiplicity as a function of $\sqrt{s}$, for both inelastic and non-single-diffractive events. Full symbols refer to this experiment. Data from other experiments are also included: circles, Ref. 8, triangles, Ref. 9, squares, Refs. 10 and 11 and diamond, Ref. 13.

in the preceding section, were applied. Comparing the multiplicity distributions for inelastic and non-single-diffractive events at the same energy, it is obvious that subtraction of diffractive events yields a nondiffractive distribution which is smaller in width and has a larger mean value than for the full inelastic distribution. We also observe the well-known increase with energy of both the width and the mean value for each distribution. The quantitative dependence in terms of moments will be discussed below.

Errors given in the figures reflect both statistical and systematic uncertainties. In the latter case they result from the correction procedure and, in addition, at low values of multiplicity, from the uncertainty in the subtraction of elastic events and in the separation of diffractive events.

A. Moments of the distributions

In the following we present a more detailed analysis of the charged multiplicity distributions in terms of their moments.

The simplest moment is the mean multiplicity $\langle n \rangle$, where

$$\langle n \rangle = \sum nP_n \ , \tag{2}$$

and P_n is the probability to produce an event with n charged particles.

The next higher moments are the dispersions D_2 and D_3 defined as

$$D_k = \langle (n - \langle n \rangle)^k \rangle^{1/k} \ . \tag{3}$$

Furthermore, for the study of the KNO scaling behavior[6] and of particle correlations we shall use the moments f_2 and $C_2 - C_5$ defined by

$$f_2 = D_2^2 - \langle n \rangle \ , \tag{4}$$

and

$$C_k = \langle n^k \rangle / \langle n \rangle^k \ . \tag{5}$$

These moments are given in Table II(a) for inelastic events and in Table II(b) for nondiffractive ones, together with the moments, f_3, γ_2 and γ_3, defined as

$$f_3 = \langle (n - \langle n \rangle)^3 \rangle - \langle 3(n - \langle n \rangle)^2 \rangle + 2\langle n \rangle \tag{6}$$

and

$$\gamma_k = \langle (n - \langle n \rangle^k \rangle / \langle n \rangle^k \ . \tag{7}$$

B. Energy dependence of $\langle n \rangle$

The energy dependence of the mean charged multiplicity $\langle n \rangle$ is expected to reflect the underlying particle-production process. For example, Feynman scaling[7] and limiting fragmentation predict an energy dependence proportional to $\ln s$.

In Fig. 3 we show the mean charged multiplicity for both inelastic and non-single-diffractive events as a function of the c.m. energy. In addition to our data points we include results from previous experiments[8-12] and a recent measurement from the SPS collider on $p\bar{p}$ interactions.[13]

As is known and can be seen from the figure, the mean charged multiplicity rises faster than logarithmically with energy both for inelastic and for nondiffractive events.

A least-squares fit to the expression

$$\langle n \rangle = A + B \ln s + C \ln^2 s \tag{8}$$

was used to represent the energy dependence of the average multiplicity for the nondiffractive events. The results of our fits are given in Table III.

C. Test of Koba-Nielsen-Olesen (KNO) scaling

Another prediction of Feynman scaling concerns the multiplicity distribution for asymptotic values of $s (s \rightarrow \infty)$.[6]

TABLE III. Fits of the energy dependence of $\langle n \rangle$ to a parametrization of the form $\langle n \rangle = A + B \ln s + C \ln^2 s$ including data at lower energies.

	A	B	C	X^2/DF
Inelastic events	0.80±0.12	0.47±0.05	0.114±0.005	1.16
Nondiffractive events, UA5 value included	0.61±0.33	0.56±0.06	0.129±0.010	2.61
Nondiffractive events, UA5 value excluded	−0.25±0.11	0.94±0.05	0.090±0.004	1.48
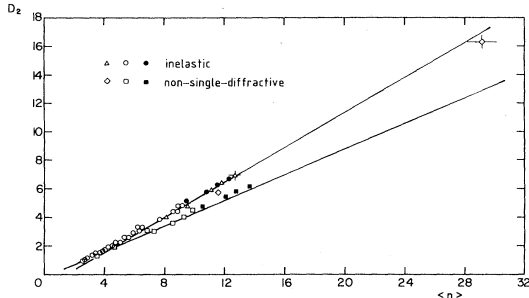
FIG. 4. D_2 moment of the charged multiplicity distribution as a function of the average multiplicity. The full symbols represent the results of this experiment. Data from other experiments are also included, diamonds, Refs. 12 and 13, otherwise as in Fig. 3.

Choosing $z = n / \langle n \rangle$ as the scaling variable, the multiplicity distribution expressed in this new variable should be independent of energy. Hence, the probability P_n to find events with n charged particles, multiplied by $\langle n \rangle$, should be described by a universal function

$$\psi(z) = \langle n \rangle P_n \ . \tag{9}$$

A test of the KNO scaling hypothesis is provided by an examination of the energy dependence of the moments of the distribution. Exact KNO scaling would, e.g., yield constant values for the moments C_k and for $D_2 / \langle n \rangle$. We therefore display in Fig. 4 the moments D_2 for inelastic and for non-single-diffractive events as a function of $\langle n \rangle$ in order to test the linear dependence.[14] The data points for both samples lie on straight lines

$$D_2 = a \langle n \rangle + b \ . \tag{10}$$

For ideal KNO scaling we expect $b = 0$ since $D_2 / \langle n \rangle$ is assumed not to depend on energy.

Fitting expression (10) to the data we found the parametrization

$$D_2 = (0.606 \pm 0.002) \langle n \rangle - (0.74 \pm 0.02)$$

for the inelastic sample and

$$D_2 = (0.439 \pm 0.007) \langle n \rangle - (0.02 \pm 0.06)$$

for the non-single-diffractive component.

The data point at the highest energy corresponding to $\langle n \rangle = 29.1$ from a measurement at the SPS $\bar{p}p$ collider[13] was not included in the fit. As can be seen from the fitted straight lines in Fig. 4, neither the inelastic nor the non-single-diffractive data extrapolate to the SPS value. This has been tentatively explained as the onset of a new production mechanism.[13]

Since the parameter b in relation (10) is close to zero and therefore $D_2 / \langle n \rangle$ is approximately constant for the sample of non-single-diffractive events, the KNO scaling seems to be fulfilled for these data, whereas the inelastic sample shows a clear deviation from scaling. This is consistent with the results on πp and Kp interactions[4] which showed that, e.g., leading-particle effects cause breaking of the KNO scaling behavior; therefore inelastic events
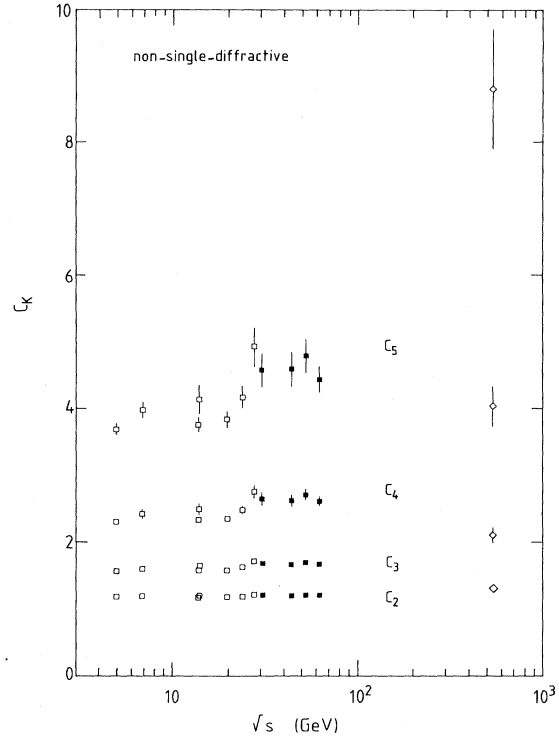
FIG. 5. The moments C_k of the charged multiplicity distribution as a function of the energy. The full symbols show the results of this experiment. Data from other experiments are also included (references as in Fig. 3).
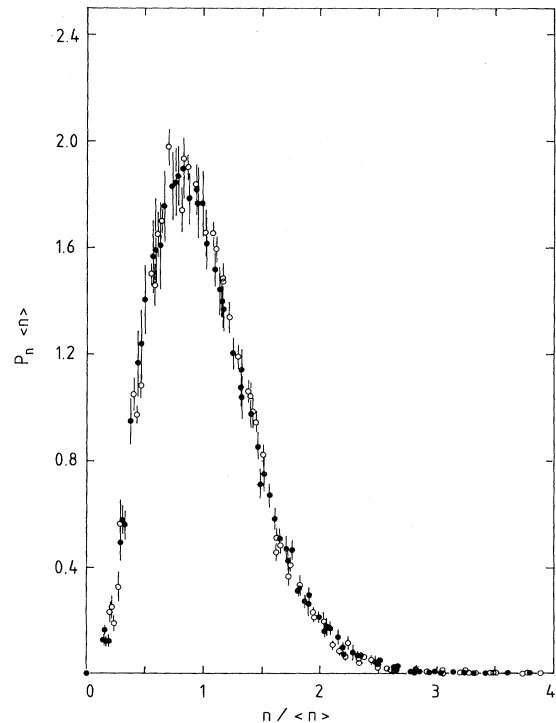
FIG. 6. Normalized multiplicity distribution of charged particles $\langle n \rangle P_n$ as a function of the KNO scaling variable $z = n / \langle n \rangle$. Data at lower energies are from experiments at Fermilab (Ref. 10). The full symbols represent the results of this experiment.

are not expected to satisfy the conditions for KNO scaling. For the further analysis we shall use non-single-diffractive events only.

The moments C_{2-5} for the non-single-diffractive events are shown in Fig. 5 as a function of energy. A slight increase is observed in passing from lower to ISR energies, but there is no evidence of an increase over the energy range of the ISR.

In Fig. 6 we display the normalized charged multiplicity distribution using only non-single-diffractive events. Data points at seven different energies[10] are superimposed and are all consistent with a universal curve within the experimental uncertainties.

D. Two-particle correlations

Uncorrelated particle production is equivalent to a Poisson multiplicity distribution. We have already observed a deviation from this hypothesis through the behavior of the moment D_2, since uncorrelated particle production would not yield the observed linear dependence of D_2 on $\langle n \rangle$. But it is the behavior of the moment f_2 which is indicative of a strong two-particle correlation.

The two-particle correlation function f_2 can be defined as

$$f_2 = \int \left[\frac{1}{\sigma_{\text{in}}} \frac{d^2\sigma}{dq_1 dq_2} - \frac{1}{\sigma_{\text{in}}} \frac{d\sigma}{dq_1} \frac{1}{\sigma_{\text{in}}} \frac{d\sigma}{dq_2} \right] dq_1 dq_2 ,$$

(11)

where σ_{in} is the inelastic cross section, $d^2\sigma/dq_1 dq_2$ is the inclusive two-particle cross section as a function of momenta q_1 and q_2, and $d\sigma/dq$ is the inclusive single-particle cross section.[15] Uncorrelated particle production in general implies $f_2 = 0$. In Fig. 7 we plot f_2 as a function of the mean charged multiplicity $\langle n \rangle$ and observe a strong two-particle correlation increasing with the mean charged multiplicity. It should be pointed out, however, that the two-particle correlations observed in inclusive studies are not only due to "true" correlations between two particles produced in the same event, but correlations are also induced by adding events of different structure, e.g., of different multiplicity.[16]

VI. CONCLUSIONS

We have presented direct measurements of the charged-particle multiplicity distributions for pp collisions at four different ISR energies. The study of various mo-
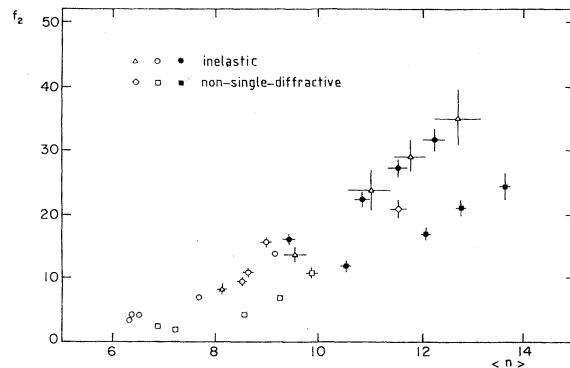
FIG. 7. Second Müller moment f_2 of the charged-particle multiplicity distribution as a function of the average multiplicity. The full symbols represent the results of this experiment. Data from other experiments are also included: diamond, Ref. 12, otherwise as in Fig. 3.

ments of the multiplicity distributions leads to the following conclusions.

(i) The energy dependence of the mean charged multiplicity may be described by an expression of the form

$$\langle n \rangle = A + B \ln s + C \ln^2 s .$$

A simple $\ln s$ dependence is excluded by the data.

(ii) The energy dependence of the dispersion $D_2 / \langle n \rangle$ is in good agreement with expectations from KNO scaling for the non-single-diffractive data whereas the scaling is broken for the sample of inelastic events. This scaling behavior is supported by the energy dependence of the moments C_{2-5} and the rescaled multiplicity distribution if one uses the non-single-diffractive events only.

(iii) Charged-particle correlations measured by the moment f_2 increase with the mean multiplicity much faster than linear. This result was observed by previous experiments,[10] and continues to the highest available energies.[13]

ACKNOWLEDGMENTS

[1]W. Bell *et al.*, Nucl. Instrum. Methods **156**, 111 (1978); M. Della Negra *et al.*, Nucl. Phys. **B127**, 1 (1977); W. Bell *et al.*, Nucl. Instrum. Methods **124**, 437 (1975).

[2]D. Drijard *et al.*, Z. Phys. C **12**, 217 (1982); B. Rensch, diploma thesis, Heidelberg, 1983.

[3]W. Herr, diploma thesis, Heidelberg, 1980; S. Jadach, Comput. Phys. Commun. **9**, 297 (1975); M. Wunsch, diploma thesis, Heidelberg, 1983.

[4]J. Dumarchez *et al.*, Nuovo Cimento **66A**, 114 (1981).

[5]U. Amaldi *et al.*, Nucl. Phys. **B166**, 301 (1980).

[6]Z. Koba *et al.*, Nucl. Phys. **B40**, 317 (1972).

[7]R. P. Feynman, Phys. Rev. Lett. **23**, 1414 (1969).

[8]E. de Wolf *et al.*, Nucl. Phys. **B87**, 325 (1975) and references therein.

[9]W. Thomé *et al.*, Nucl. Phys. **B129**, 365 (1977).

[10]J. Whitmore *et al.*, Phys. Rep. **10C**, 273 (1974); S. Barish

et al., Phys. Rev. D **9**, 2689 (1974); C. Bromberg *et al.*, Phys. Rev. Lett. **31**, 1563 (1973); A. Firestone *et al.*, Phys. Rev. D **10**, 2080 (1974).

[11]J. Benecke *et al.*, Nucl. Phys. **B76**, 29 (1974); W. M. Morse *et al.*, Phys. Rev. D **15**, 66 (1977).

[12]K. Alpgard *et al.*, Phys. Lett. **112B**, 183 (1982).

[13]K. Alpgard *et al.*, Phys. Lett. **121B**, 209 (1983); G. J. Alner *et al.*, UA5 Collaboration, report, 1983 (unpublished); K. Böckmann, UA5 Collaboration, presented at the 3rd International Conference on Physics in Collisions, Como, Italy, 1983 (unpublished).

[14]A. Wroblewski, Acta Phys. Pol. **43**, 857 (1973).

[15]A. H. Müller, Phys. Rev. D **4**, 150 (1971).

[16]W. Bell *et al.*, Report No. CERN/EP83-149 (unpublished).